

TABLE 5. CORRELATIONS OF MICROSTRUCTURAL PARAMETERS BY MDCT WITH AGE OR BODY WEIGHT

	<i>Vs. age (years)</i>		<i>Vs. body weight (kg)</i>	
	<i>R</i> ²	<i>p</i>	<i>R</i> ²	<i>p</i>
Microstructure parameters				
App BV/TV (%)	0.114	0.0005	0.029	NS
App Tb.N (1/mm ³)	0.122	0.005	0.147	0.0005
App Tb.Th (μm)	0.099	0.005	0.030	NS
App Tb.Sp (μm)	0.081	0.01	0.125	0.005
Structure model index	0.181	0.0001	0.048	0.05
Euler's number	0.185	0.0001	0.068	0.05
Fractal dimension	0.049	0.05	0.030	NS
Degree of anisotropy	0.005	NS	0.130	0.001
BMD				
Areal BMD by DXA (g/cm ²)	0.091	0.01	0.072	0.05
Volumetric BMD by MDCT (mg/cm ³)	0.118	0.005	0.001	NS

app BV/TV, apparent bone volume fraction; app Tb.N, apparent trabecular number; app Tb.Th, apparent trabecular thickness; app Tb.Sp, apparent trabecular separation; NS, not significant.

fracture.⁽²¹⁾ A disadvantage of high-resolution MRI *in vivo*, however, is the relatively long acquisition time of up to 10 ± 20 minutes. A small FOV is required to obtain a high signal-to-noise ratio in the fast gradients with optimized coils. Because of these prerequisites and motion artifacts in the axial skeleton, application of high-resolution MRI is currently limited to peripheral sites such as phalanges, calcaneus, and distal radius.^(19,20,25–27) Vertebral fracture is the most common osteoporotic fracture, and the presence of fracture indicates a greater risk for future fracture, independently of BMD.⁽²⁸⁾ The direct assessment of vertebral microstructure, as reported here, can be expected to provide greater sensitivity for assessing the risk of spinal fracture.

To our knowledge, there has been no report on *in vivo* analysis of microstructure by MDCT. Several specimen studies showed the capability to depict microstructure by MDCT in comparison with contact radiography⁽¹⁶⁾ or μCT.⁽¹⁷⁾ Although MDCT is the only available technique to analyze vertebral microstructure *in vivo*, high radiation exposure cannot be avoided. The radiation dose for DXA is small (0.08 ± 4.6 mSv). Fan beam DXA with increased resolution requires an increased radiation dose (6.7 ± 31 mSv), but this dose is smaller than that for QCT (25 ± 360 mSv).⁽²⁹⁾ In a study comparing radiation doses between single-detector row CT and MDCT, a 28% higher radiation dose was needed within the scanned volume for the latter at a constant noise level.⁽³⁰⁾ In this study, we evaluated the image quality of trabecular microstructure as a function of radiation exposure dose by using excised human vertebrae. Within the limits of clinically available radiation sets, MDCT at 300 mAs provided the best image quality and showed the highest correlation with the μCT data. As the reference level for CT examination of the abdomen (CTDI_w) of adult patients is 35 mGy (according to European Commission 1999), the CTDI_w for our current MDCT scanning at 300 mAs was 77.1 mGy. This radiation dose would be acceptable for a once-a-year study on postmenopausal women. On further advancement of the technology, a reduction in the radiation dose and higher reso-

lution with a higher signal-to-noise ratio would be expected to make this method an even more useful diagnostic tool. In fact, the CTDI_w for a new 16-detector row CT apparatus is 19.7 mGy, and advanced CT technology is expected to provide higher-resolution CT images. In the future, finite element analysis (FEA) may also be applied to 3D MDCT data for assessment of biomechanical properties,^(31,32) and together this combination should provide a powerful tool for early evaluation of fracture risk.

In conclusion, 3D imaging of trabecular microstructure can be performed by using clinical MDCT at a high spatial resolution, and microstructure parameters derived from these images, especially those related to the shape of trabecular structures and connectivity, are more useful than spinal DXA for the assessment of fracture risk.

ACKNOWLEDGMENTS

The authors thank Tomoko Nakata and Takako Shimogama (Division of Radiology, Nagasaki University Hospital) and Jun Kono (Department of Radiology, Nagasaki Saiseikai Hospital) for CT scanning and analysis of trabecular structure. This work was supported in part by the Program for Promotion of Fundamental Studies in Health Science from Pharmaceuticals and Medical Device Agency (Pmda) of Japan (MF-14 to MI) and by a Health and Labour Sciences Research Grant (Comprehensive Research on Aging and Health) from the Ministry of Health, Labour and Welfare of Japan (to MI and HO).

REFERENCES

1. Siris ES, Chen Y-T, Abbott TA, Barrett-Connor E, Miller PD, Wehren LE, Berger MC 2004 Bone mineral density thresholds for pharmacological intervention to prevent fractures. *Arch Intern Med* 164:1108–1112.
2. Riggs BL, Melton LJ 2002 Bone turnover matters: The raloxifene treatment paradox of dramatic decreases in vertebral fractures without commensurate increases in bone density. *J Bone Miner Res* 17:11–14.

3. Seeman E 2002 Pathogenesis of bone fragility in women and men. *Lancet* **359**:1841–1850.
4. Chevalier F, Laval-Jeantet A, Laval-Jeantet M, Bergot C 1992 CT image analysis of the vertebral trabecular network in vivo. *Calcif Tissue Int* **51**:8–13.
5. Link TM, Majumdar S, Lin J, Augat P, Gould R, Newitt D, Ouyang X, Lang T, Mathur A, Genant HK 1998 Assessment of trabecular structure using high-resolution CT images and texture analysis. *J Comput Assist Tomogr* **22**:15–24.
6. Ito M, Ohki M, Hayashi K, Yamada M, Uetani M, Nakamura T 1995 Trabecular texture analysis of CT images in the relationship with spinal fracture. *Radiology* **194**:55–59.
7. Ruegsegger P, Koller B, Mueller R 1996 A microtomographic system for the non-destructive evaluation of bone architecture. *Calcif Tissue Int* **58**:24–29.
8. Mueller R, Hahn M, Vogel M, Delling G, Ruegsegger P 1996 Morphometric analysis of non-invasively assessed bone biopsies: Comparison of high-resolution computed tomography and histologic sections. *Bone* **18**:215–220.
9. Hildebrand T, Ruegsegger P 1997 A new method for the model-independent assessment of thickness in three-dimensional images. *J Microsc* **185**:67–75.
10. Parfitt AM, Drezner MK, Glorieux FH, Kanis JA, Malluche H, Meunier PJ, Ott SM, Recker RR 1987 Bone histomorphometry: Standardization of nomenclature, symbols, and units. Report of the ASBMR Histomorphometry Nomenclature Committee. *J Bone Miner Res* **2**:595–610.
11. Fazzalari NL, Parkinson IH 1996 Fractal dimension and architecture of trabecular bone. *J Pathol* **178**:100–105.
12. Odgaard A, Gundersen HJ 1993 Quantification of connectivity in cancellous bone, with special emphasis on 3-D reconstructions. *Bone* **14**:173–182.
13. Harrigan TP, Mann RW 1984 Characterization of microstructural anisotropy in orthotropic materials using a second rank tensor. *J Mater Sci* **19**:761–767.
14. Genant HK, Wu CY, vanKuijk C, Nevitt M 1994 Vertebral fracture assessment using a semi-quantitative technique. *J Bone Miner Res* **8**:1137–1148.
15. Gordon CL, Lang TF, Augat LP, Genant HK 1998 Image-based assessment of spinal trabecular bone structure from high-resolution CT images. *Osteoporos Int* **8**:317.
16. Link TM, Vieth V, Stehling C, Lotter A, Beer A, Newitt D, Majumdar S 2003 High-resolution MRI vs multislice spiral CT: Which technique depicts the trabecular bone structure best? *Eur Radiol* **13**:663.
17. Issever AS, Vieth V, Lotter A, Meier N, Laib A, Newitt D, Majumdar S, Link TM 2002 Local differences in the trabecular bone structure of the proximal femur depicted with high-spatial-resolution MR imaging and multisection CT. *Acad Radiol* **9**:1395.
18. Gordon CL, Webber CE, Christoforou N, Nahmias C 1997 In vivo assessment of trabecular bone structure at the distal radius from high-resolution magnetic resonance images. *Med Phys* **24**:585–593.
19. Majumdar S, Genant HK, Grampp S, Newitt DC, Truong V-H, Lin JC, Mathur A 1997 Correlation of trabecular bone structure with age, bone mineral density and osteoporotic status: In vivo studies in the distal radius using high resolution magnetic resonance imaging. *J Bone Miner Res* **12**:111–118.
20. Link TM, Majumdar S, Augat P, Lin JC, Newitt D, Lu Y, Lane NE, Genant HK 1998 In vivo high resolution MRI of the calcaneus: Differences in trabecular structure in osteoporosis patients. *J Bone Miner Res* **13**:1175–1182.
21. Majumdar S, Link TM, Augat P, Lin JC, Newitt D, Lane NE, Genant HK 1999 Trabecular bone architecture in the distal radius using magnetic resonance imaging in subjects with fractures of the proximal femur. *Osteoporos Int* **10**:231–239.
22. Majumdar S, Kothari M, Augat P, Newitt DC, Link TM, Lin JC, Lang T, Lu Y, Genant HK 1998 High-resolution magnetic resonance imaging: Three-dimensional trabecular bone architecture and biomechanical properties. *Bone* **22**:445–454.
23. Majumdar S, Newitt D, Mathur A, Osman D, Gies A, Chiu E, Lotz J, Kinney J, Genant H 1996 Magnetic resonance imaging of trabecular bone structure in the distal radius: Relationship with X-ray tomographic microscopy and biomechanics. *Osteoporos Int* **6**:376–385.
24. Wehrli F, Hwang S, Ma J, Song H, Ford J, Haddad J 1998 Cancellous bone volume and structure in the forearm: Noninvasive assessment with MR microimaging and image processing. *Radiology* **206**:347–357.
25. Lin J, Amling M, Newitt D, Selby K, Delling G, Genant H, Majumdar S 1996 Heterogeneity of trabecular bone structure in the calcaneus using high resolution magnetic resonance imaging (MRI). *Osteoporos Int* **8**:16–24.
26. Link T, Majumdar S, Lin J, Newitt D, Augat P, Ouyang X, Mathur A, Genant H 1998 A comparative study of trabecular bone properties in the spine and femur using high resolution MRI and CT. *J Bone Miner Res* **13**:122–132.
27. Kuehn B, Stampa B, Heller M, Glueer C 1997 In vivo assessment of trabecular bone structure of the human phalanges using high resolution magnetic resonance imaging. *Osteoporos Int* **7**:291.
28. Ross PD, Genant HK, Davis JW, Miller PD, Wasnich RD 1993 Predicting vertebral fracture incidence from prevalent fractures and bone density among non-black, osteoporotic women. *Osteoporos Int* **3**:120–126.
29. Njeh CF, Fuerst T, Hans D, Blake GM, Genant HK 1999 Radiation exposure in bone mineral density assessment. *Appl Radiat Isot* **50**:215.
30. Thornton FJ, Paulson EK, Yoshizumi TT, Frush DP, Nelson RC 2003 Single versus multi-detector row CT: Comparison of radiation doses and dose profiles. *Acad Radiol* **10**:379.
31. van Rietbergen B, Weinans H, Huiskes R, Odgaard A 1995 A new method to determine trabecular bone elastic properties and loading using micromechanical finite-element models. *J Biomech* **28**:69–81.
32. Ito M, Nishida A, Koga A, Ikeda S, Shiraishi A, Uetani M, Hayashi K, Nakamura T 2002 Contribution of trabecular and cortical components to the mechanical properties of bone and their regulating parameters. *Bone* **31**:351–358.

Address reprint requests to:
 Masako Ito, MD
 Division of Radiology
 Nagasaki University Hospital
 Nagasaki 852-8501, Japan
 E-mail: masako@net.nagasaki-u.ac.jp

Received in original form February 16, 2005; revised form June 4, 2005; accepted June 16, 2005.

Ataxia telangiectasia mutated (*Atm*) knockout mice as a model of osteopenia due to impaired bone formation

Akinori Hishiya^a, Masako Ito^b, Hiroyuki Aburatani^c, Noboru Motoyama^d,
Kyoji Ikeda^a, Ken Watanabe^{a,*}

^aDepartment of Bone and Joint Disease, National Institute for Longevity Sciences (NILS), National Center for Geriatrics and Gerontology (NCGG),
36-3 Gengo, Morioka-cho, Obu, Aichi 474-8522, Japan

^bDepartment of Radiology, Nagasaki University Hospital, Nagasaki, Japan

^cDepartment of Cancer Systems Biology, Research Center for Advanced Science and Technology, The University of Tokyo, Tokyo, Japan

^dDepartment of Geriatric Medicine, NCGG, Obu, Japan

Received 19 December 2004; revised 11 April 2005; accepted 20 May 2005

Available online 18 July 2005

Abstract

ATM is a member of the PI-3 kinase protein family, encoded by the gene, *ATM*, responsible for ataxia telangiectasia (AT). AT is recognized as a genomic instability syndrome, sharing accelerated senescence symptoms in human and mouse. Here, we present evidence that the bone phenotype of *Atm* knockout (AtmKO) mice is similar to that observed in disuse and/or aging syndromes. A significant decrease in 3-dimensional bone volume fraction (BV/TV) of the fifth lumbar vertebra was observed in AtmKO mice by μ CT, compared with heterozygous control mice at 10 weeks of age. Bone histomorphometry revealed that both BFR/BS and Oc.S/BS were significantly decreased in KO mice. To determine the cellular basis of this bone phenotype, we employed in vitro osteoclastogenesis and colony formation assays using bone marrow cells derived from KO and control mice. There was no difference in osteoclast formation in ex vivo cultures. CFU-F was markedly reduced in AtmKO-derived cultures compared with control mice, whereas differentiation of calvaria-derived osteoblasts did not differ between the genotypes. Furthermore, expression levels of IGF1R were significantly decreased, and p38 was aberrantly phosphorylated in marrow stromal cells from AtmKO mice. These results indicate that the pathogenesis of the osteopenic phenotype in AtmKO mice is similar to that of disuse and/or aging syndromes and is caused, at least in part, by a stem cell defect due to lack of IGF signaling.
© 2005 Elsevier Inc. All rights reserved.

Keywords: Premature aging syndrome; Animal models; Mesenchymal stem cells; Knockout

Introduction

Much progress has been achieved in our understanding of the pathogenesis of postmenopausal osteoporosis, characterized by accelerated bone resorption [1,2]. On the other hand, the pathophysiology of senile osteoporosis, caused mainly by declining bone-forming capacity, remains an enigma due to the lack of suitable animal models. Although aged (2 to 3 years old) animals are good candidates, natural aging is a complex phenomenon involving a plethora of

factors and is difficult to dissect at the molecular level. Recently, genetically engineered mouse models for studying aging and age-related disorders have been developed [3]. Since they are caused by single gene mutations, they provide valuable tools for studying the pathogenesis of senile osteoporosis at the molecular level. For example, osteopenia with reduced bone formation and resorption has been reported in *klotho* (*kl/kl*) and mutant p53-expressing mice [4,5].

Ataxia telangiectasia (AT) is a human premature aging syndrome characterized by neurodegeneration, immune defects, tumor formation, hypersensitivity to ionizing radiation, and genomic instability [6]. The responsible gene, *ATM* (for AT mutated), is a large protein kinase that belongs

* Corresponding author. Fax: +81 562 44 6595.

E-mail address: kwatanab@nils.go.jp (K. Watanabe).

to the PI-3 kinase family [10,11]. ATM functions in DNA damage checkpoint and oxidative stress responses, thereby playing a central role in the maintenance of genome stability. Mouse models for AT have been generated by knockout of the mouse *Atm* gene [7–9]. *Atm*KO mice exhibit radiosensitivity, genomic instability, growth retardation, and lymphoma, recapitulating main features of human AT [7–9]. The bone phenotype, however, has not been defined. Interestingly, mice deficient in *Abl*, a downstream protein kinase effector of ATM, exhibit an osteopenic phenotype with reduced bone formation [27]. We report here that *Atm*KO mice show osteopenia as early as 10 weeks of age, when growth retardation is not apparent. Histomorphometric and biochemical analyses revealed impaired bone formation, which may be caused by limited proliferative potential of osteogenic progenitors. Thus, *Atm*KO mice may provide a suitable model for studying senile osteoporosis.

Materials and methods

Mice

*Atm*KO mice (129/SvEv-*Atm*^{tm1Awb}) were obtained from Jackson Labs (Bar Harbor, Maine, USA). All generations were from matings of heterozygous parents. Genotyping was performed as described [9,12] with the exception of the primers used to detect the wild type allele. The primer sequences used for genotyping were as follows:

oIMR640, 5'-GCTGCCATACTTGATCAATG-3'
oIMR641, 5'-TCCGAATTTGCAGGAGTTG-3'.

The sequences used were recommended by Jackson Labs. All animal experiments were approved in advance by the Ethics Review Committee for Animal Experimentation of the National Institute for Longevity Sciences and the National Center for Geriatrics and Gerontology.

Bone morphological and histomorphometric analyses

Lumbar vertebrae and tibias were obtained from 6-, 10-, and 14-week-old female and male mice and subjected to morphological analyses ($n = 3 \sim 6$). Microcomputed tomography (μ CT) and bone histomorphometry of the vertebrae and tibias, respectively, doubly labeled by calcein, were performed as described previously [13].

CFU assay

Colony forming unit (CFU) assays were conducted according to Jilka et al. [14]. Briefly, bone marrow cells were obtained from femurs or tibias and seeded at 1.5×10^6 (for CFU-F/CFU-ALP) or 2.5×10^6 (for CFU-Ob or CFU-Adip) cells/well in a 6-well plate. For CFU-F and CFU-Ob,

the marrow cell cultures were maintained in phenol red-free α MEM containing 15% FCS and 1 mM Asc-2-P; one-half of the medium was replaced every 5 days. For CFU-Adip, the cultures were maintained in phenol red-free α MEM (Invitrogen, Carlsbad, California, USA) containing 15% FCS and MDI (0.5 mM methylisobutylxanthine, 1 μ M dexamethasone, 1 μ g/ml insulin) for 25–28 days. The cells were cultured for 10 days and then stained for ALP and counterstained with hematoxylin. Colonies of cells containing a minimum of 20 cells were designated as CFU-F, and those positive for ALP activity as CFU-ALP. For CFU-Ob, the cells were maintained for 25–28 days, fixed in 50% ethanol and 18% formaldehyde, and then stained using 2% Alizarin Red. The oil drops in the adipocytic cells were stained by Oil Red-O.

Osteoblastic cell cultures

Osteoblastic cells were isolated from calvarias of neonatal (P2–P3) *Atm*KO or wild-type mice following the protocol described by Jochum et al. [15] with minor modifications. For alkaline phosphatase (ALP) staining, osteoblastic cells were cultured in 24-well tissue culture plates. After reaching confluency, medium was supplemented with 60 μ g/ml ascorbic acid and 10 nM dexamethasone and cultured for 7 more days. ALP staining was performed using a leukocyte alkaline phosphatase staining kit (SIGMA Diagnostics, St. Louis, USA). For ALP activity measurement, cells from the same conditions described above were washed with PBS and sonicated in RIPA buffer (50 mM Tris-HCl (pH 7.5) containing 150 mM NaCl, 1% NP-40, 0.5% sodium deoxycholate, and 0.1% sodium dodecyl sulfate). ALP activity in the lysate was measured using an ALP activity measurement kit (Wako Pure Chemical Industries, Osaka, Japan). The protein content was determined using BCA protein assay reagent (Pierce Chemical Co., Rockford, Illinois, USA).

M-CSF-dependent cell proliferation assay

Bone marrow cells were isolated from *Atm*KO or control mice, and the erythrocytes in the collected cells were depleted by standard ammonium-chloride lysis. To assess M-CSF-dependent proliferative response, cells (3×10^4) were cultured in flat-bottom 96-well plates for 2 days with various amounts of M-CSF (R&D Systems, Minneapolis, USA). Cultures were pulsed for 24 h with 1 μ Ci/well of [³H]thymidine, harvested on glass-fiber filters, and the incorporated radioactivity was determined using a beta counter.

In vitro osteoclastogenesis assay

Bone marrow cells were isolated from *Atm*KO or control mice and incubated in tissue culture plates with α MEM containing 10% FCS. After 4 h in culture, nonadherent cells

were collected and counted. 5×10^5 cells were cultured for 3 days in 24-well tissue culture plates with 10 ng/ml M-CSF and for an additional 3 days in the presence of both 10 ng/ml M-CSF and 10 ng/ml RANKL (R&D Systems). Adherent cells were then fixed with an acetone–citrate–formalin solution (65:27:7) and stained for TRAP using a leukocyte acid phosphatase kit (SIGMA Diagnostics). The number of TRAP-positive multinucleated cells containing more than three nuclei was counted as osteoclasts.

Immunoblot analysis

Adherent cells from bone marrow of AtmKO or control mice were lysed in RIPA buffer containing 2 mM phenyl–methyl–sulfonyl fluoride, 10 mM sodium fluoride, 2 mM sodium vanadate, and proteinase inhibitor cocktail (Complete™, Roche Diagnostics, GmbH Mannheim, Germany). The cell lysates (15 µg each of protein) were subjected to SDS-PAGE, transferred, and then detected with antibodies using ECL-Plus (Amersham-Pharmacia). Anti-p38 (sc-535), anti-IGF1R (sc-713), and anti-c-Abl (sc-131) antibodies were purchased from Santa Cruz Biotechnology, California, USA. Anti-phosphorylated p38 (9211) and anti-tubulin (T5168) were obtained from Cell Signaling Technology (Beverly, Massachusetts, USA) and SIGMA, respectively.

IGF-dependent cell proliferation assay

Bone marrow cells were obtained as described above. The adherent cells were harvested and replated at a density of 5×10^4 cells/well in 96-well plates. After 24-h serum deprivation, the cultures were labeled with [3 H]thymidine with or

without human recombinant IGF-I (10 ng/ml; Invitrogen). The incorporated [3 H] was measured as described.

Statistical analysis

Data are presented as mean \pm SD. All data were analyzed by Student's *t* test. Statistical significance was considered at $P < 0.05$, unless otherwise indicated.

Results

Osteopenia due to impaired bone formation in AtmKO mice

To characterize the bone phenotype of Atm homozygous knockout mice with heterozygous littermates as controls, μ CT scanning technique was employed. We analyzed 6-, 10-, and 14-week-old animals. At 6 weeks of age, there was no significant decrease in bone mass of AtmKO mice (data not shown). Since ovarian defect, which was possible to affect bone metabolism, was observed in female KO mice [7–9], we focused in the structural data from male animals. As shown in Figs. 1A and B, 3-dimensional bone volume (BV/TV) of the lumbar vertebrae was markedly decreased in AtmKO mice at 10 weeks of age. At this age, there is no significant difference in body weight between AtmKO and littermate control mice (24.8 ± 1.6 versus 21.5 ± 2.4 g). The trabecular number (Fig. 1C) and thickness (Fig. 1D) were also reduced in AtmKO mice compared to control. The difference between KO and control mice was more pronounced at age of 14 weeks, when some KO animals became cachexic.

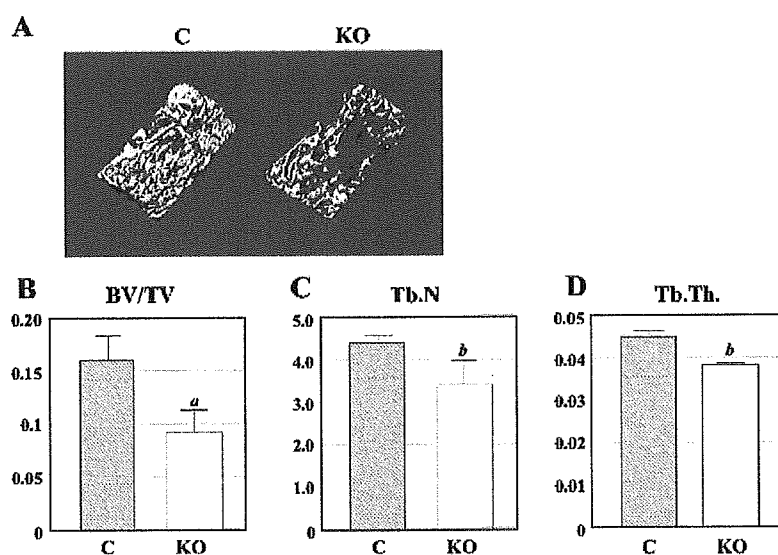


Fig. 1. Micro-CT analysis of lumbar vertebrae of AtmKO mice. The fifth lumbar vertebra from heterozygous (C) and knockout (KO) mice were subjected to μ CT analysis at 10 weeks of age. (A) Representative 3D images of trabecular architectures are shown. Note that the osteopenic phenotype was observed in knockout mice. (B) Trabecular bone volume fraction (BV/TV); (C) trabecular number (Tb.N); (D) trabecular thickness (Tb.Th.). The data were obtained in male mice. ^a $P < 0.005$ and ^b $P < 0.05$, significantly different from the respective heterozygous control group.

Bone histomorphometric analysis of the proximal tibia showed that bone formation rate (BFR/BS) and the osteoblast surface (Ob.S/BS) were significantly decreased in both female and male *Atm*KO mice (Fig. 2). The osteoclast surface (Oc.S/BS) was also reduced in the KO mice, suggesting that both bone formation and resorption were suppressed in *Atm*KO mice and that the observed osteopenic phenotype was caused mainly by impaired bone formation.

Cellular basis of impaired bone formation

To determine whether impaired bone formation was due to a cell autonomous defect, in vitro osteoblastogenesis assays were performed. The number of CFU-F (Fig. 3A), CFU-ALP (Fig. 3B), and CFU-OB (data not shown) were significantly reduced in the bone marrow of *Atm*KO mice. The decrease in CFU-F, which reflects the number and/or proliferative potential of mesenchymal progenitors, suggested that the defect was not specific to the osteoblastic lineage but involved other lineages as well. In fact, the number of CFU-adipocyte was also reduced (data not shown). We performed osteoblastogenesis assays in the presence of *N*-acetyl cysteine (NAC) to reduce oxidative stress, which often affects cell proliferation and induces senescence of primary cultured murine cells. As shown in Figs. 3A and B, supplementation with NAC increased the number of CFU-F and CFU-ALP in bone marrow cultures from control mice, but not in cultures from *Atm*KO mice. Notably, the ratio of CFU-ALP to CFU-F was not markedly altered between the genotypes, suggesting that differentiation, especially the ability to differentiate into osteoblasts, was not impaired in *Atm*KO mice.

To address the question whether the absence of *Atm* affected the differentiation process, osteoblasts were isolated from calvarias of homozygous and heterozygous knockout mice and cultured in vitro. As shown in Fig. 3C, calvaria-derived osteoblastic cells differentiated at comparable levels, suggesting that the differentiation potential of osteoblasts was not impaired in *Atm*KO mice. Together, with results from the CFU assays, these data collectively

suggested that the impaired bone formation was not due to a defect in the differentiation program of osteoblasts per se but to the proliferative potential of mesenchymal progenitors.

As for the hematopoietic lineage, M-CSF-dependent proliferation of bone marrow cells from *Atm*KO mice did not differ from that of control mice (Fig. 4A). When osteoclastogenic potential was assessed in bone marrow cultures with M-CSF and RANKL, neither the number of TRAP-positive multinucleated cells formed (Fig. 4B) nor their morphology (Fig. 4C) differed between the genotypes.

Reduced IGF1 receptor with activation of p38 in *Atm*-deficient marrow stromal cells

To gain some insight into the molecular mechanism underlying the impaired proliferation of mesenchymal progenitors in *Atm*KO mice, the expression of molecules involved in ATM signaling was analyzed by immunoblotting. As shown in Fig. 5 (right lane), the level of phosphorylated p38MAPK (P-p38) was elevated in marrow stromal cells derived from *Atm*KO mice, while the total amount of p38 in the experimental and control cultures did not differ. By contrast, the expression of IGF-I receptor (IGFIR) was markedly reduced in *Atm*KO-derived marrow stromal cells compared with control cells (Fig. 5A). The level of Abl, a downstream effector molecule involved in the ATM pathway, did not differ between the genotypes. Next, we determined whether the IGF response was impaired in cells derived from *Atm*KO mice. As shown in Fig. 5B, control cells responded to IGF with increased proliferation, whereas the response to IGF was severely impaired in the stromal cells from *Atm*KO mice, suggesting that a decline in the expression level of IGF1R causes IGF-dependent proliferation in *Atm*KO mice.

Discussion

In the present study, we demonstrate that *Atm*KO mice show reduced bone formation due to a proliferative defect in

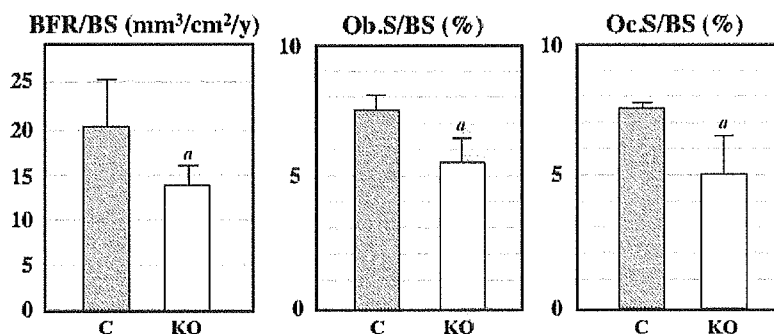


Fig. 2. Bone histomorphometric analysis of *Atm*KO mice. Decreases in bone formation rate (BFR/BS, left), osteoblast surface (Ob.S/BS, center), and osteoclast surface (Oc.S/BS, right) were measured from the proximal tibias of male *Atm*KO (KO) mice and compared with heterozygous (C) littermate controls. Data expressed are the means \pm SD. ^a*P* < 0.05, significantly different from the respective heterozygous control group.

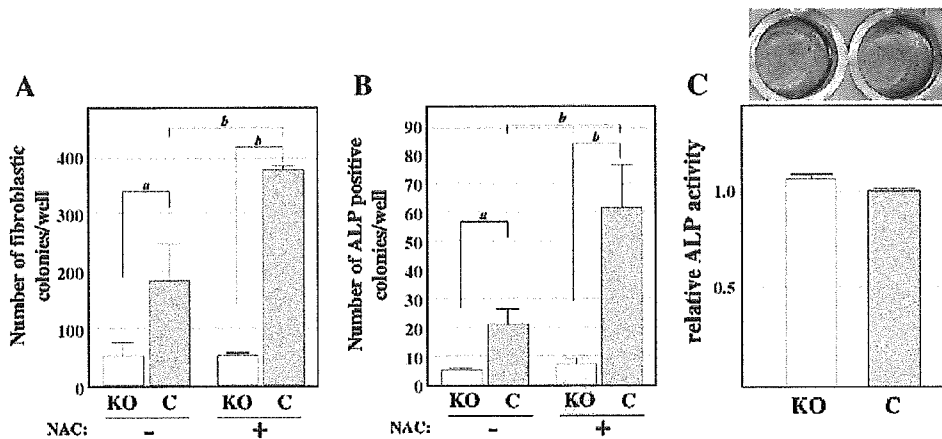


Fig. 3. Colony formation assay of bone marrow cells and calvarial osteoblast differentiation. (A) CFU-F in bone marrow cells derived from *Atm*KO (KO) or littermate wild-type or heterozygous control (C) mice ($n = 3\sim 5$) are shown. (B) CFU-ALP. Note the significant reductions in both CFU-F and CFU-ALP ($P < 0.05$, KO versus control). *N*-acetyl cysteine (NAC, 10 mM) improved the numbers of CFU-F and CFU-ALP in control but not in cells from *Atm*KO mice. (C, upper panel) A representative photograph of the wells stained for ALP activity. Lower panel, relative ALP of calvarial cell cultures. No significant difference in morphology or ALP activity was observed between knockout (KO) and controls (C). Data represent the means \pm SD. ^a $P < 0.05$ and ^b $P < 0.005$, significantly different from the respective control group. No significant difference was detected in the presence or absence of NAC in KO cells either in CFU-F or CFU-ALP assays.

mesenchymal progenitor cells, in addition to other age-related disorders observed in the human syndrome, AT, including neurodegeneration, immune defects, tumor formation, and genomic instability [7–9]. It has been suggested that, in mice as well as in humans, age-related decline in osteoblast number and function is caused by a decrease in number and proliferative potential of mesenchymal stem cells [16–19]. *Atm*KO mice recapitulate these cellular defects as early as 10 weeks of age. At this age, there are no signs of lymphoma or severe growth retardation in KO mice [7], suggesting that the bone phenotype is not caused by the secondary effects of those defects. The difference in bone mass between genotypes was more pronounced with age. The loss of bone mass associated with age may be accelerated by other abnormalities, such as growth retardation, lymphoma, immune defects, and

cachexia. Importantly, we have shown in this study that the bone marrow cells exhibited a cell autonomous defect in proliferation. Therefore, it is suggested that the impairment in bone formation with a proliferative defect in bone marrow stem cells causes the osteopenic phenotype in *Atm*KO mice, although we cannot exclude the possibility that the defects such as T-lymphopenia and hypogonadism affected the bone phenotype of more aged mice. The microstructural alterations in the lumbar vertebrae of *Atm*KO mice are also similar to those observed in naturally aging C57BL/6J mice [20]. Thus, *Atm*KO mice may provide a suitable model to study the pathophysiology of senile osteoporosis without the necessity of raising them for 2 to 3 years.

Recently, Bonyadi et al. reported that *Sca1* KO mice develop an age-dependent osteopenia [21]. *Sca1* KO mice exhibit a decrease in the number of osteoprogenitors as well

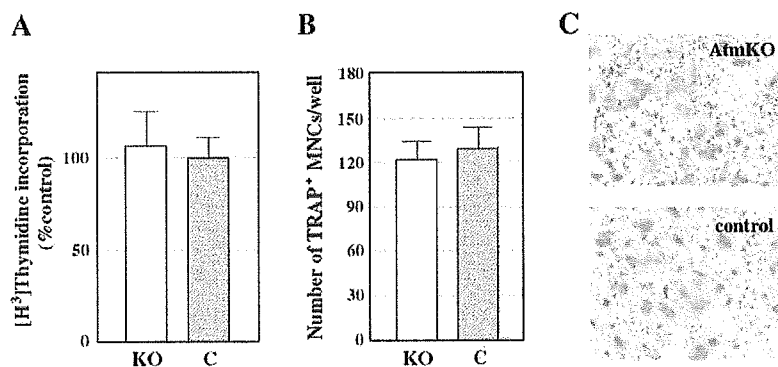


Fig. 4. M-CSF-dependent proliferation and in vitro osteoclastogenesis of bone marrow cells. (A) No obvious difference in M-CSF-dependent [³H]thymidine incorporation into bone marrow cells was detected. (B) The number of multinucleated TRAP-positive cells derived from bone marrow cells in the presence of RANKL and M-CSF. No significant difference between the cells from *Atm*KO (KO) and littermate control (C) mice was observed. (C) TRAP staining of the in-vitro-generated multinucleated cells.

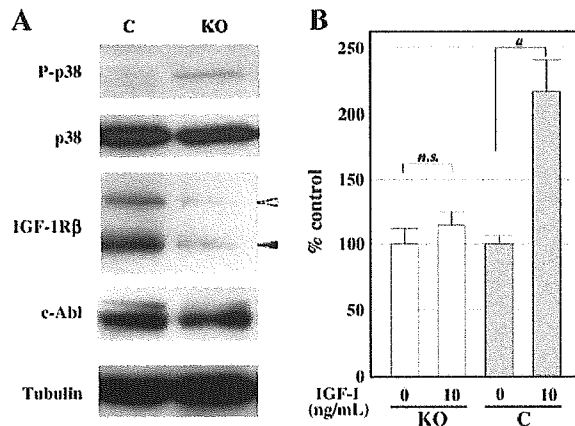


Fig. 5. Expression analysis of IGF-1 receptor in bone marrow cells. (A) Total cell lysates of bone marrow stromal cells from wild-type (C, left lane) or *Atm* knockout (KO, right lane) were subjected to immunoblot analyses. Top panel (P-p38), activated (phosphorylated) p38. Second panel (p38), total p38 MAP kinase. The activated p38 is only detected in *Atm*KO. These two panels were from a membrane blot. Third panel (IGF-1R β), probed with antibody against the insulin-like growth factor receptor β subunit. The upper (open arrowhead) and lower (closed arrowhead) bands correspond to unprocessed and processed β subunit protein, respectively. Fourth panel (c-Abl) shows expression level of c-Abl protein. The bottom panel, probed with anti-tubulin antibody to control for protein loading in the last three panels (IGF-1R β , c-Abl). (B) IGF-I response. Bone marrow stromal cells from *Atm* knockout (KO) or wild-type (C) were cultured with or without IGF-I. Incorporated thymidine was measured and displayed as fold change (%) compared to culture without IGF for each genotype. ^a $P < 0.005$; n.s., not significant.

as CFU-F and have a non-cell autonomous defect in osteoclasts [21]. Although defects of osteoblasts and osteoclasts are similarly observed in *Atm*KO mice, the expression of *Sca1* mRNA was not altered in *Atm*KO mice (data not shown). Additionally, the onset of the bone phenotype in *Sca1* KO (~12 months of age) was very late, compared with that of *Atm*KO mice (~10 weeks). Thus, the impact of ATM deficiency on bone formation was more severe than that of *Sca1* deficiency.

It has been reported that *Atm*KO mice showed reduced numbers of leukocytes in the circulation as well as bone marrow [7–9,22]. Although osteoclast surface was reduced in the bone of *Atm*KO mice, osteoclastogenic potential as well as M-CSF-dependent cell proliferation in vitro was normal, pointing to the involvement of impaired ability of the marrow environment to support proliferation/differentiation of osteoclast progenitors rather than cell autonomous dysfunction in the hematopoietic lineage. Concerning the osteoblastic lineage of *Atm*KO mice, the defect lies mainly in CFU-F, while the differentiation of osteoblasts was rather normal. Thus, it is tempting to speculate that multi-potent stem or progenitor cells are more sensitive to *Atm* deficiency than are differentiated cells. As we did not find any difference in the expression of Jagged-1 (data not shown), one of the key molecules that function in the bone marrow niche [23], the molecular defect in niche function of *Atm*KO mice remains to be clarified.

Chk2 is a checkpoint kinase that functions downstream of ATM and phosphorylates p53 to stabilize it [11,24]. Soft X-ray analysis of bones from *Chk2* KO mice [25] revealed no alteration in bone density (AH et al., unpublished observation). It has been reported that the bones of mice lacking p53, the target of ATM and *Chk2* kinases, were normal, although they were resistant to bone loss in response to unloading [26]. Thus, it is unlikely that the *Chk2* pathway is involved in the impaired bone formation in *Atm*KO mice.

It has been reported that mice lacking *Abl*, another downstream kinase of ATM, exhibit an osteopenic phenotype due to reduced bone formation, which is caused mainly by a defect in osteoblast differentiation [27]. In *Atm*KO mice, by contrast, osteoblastic differentiation is normal. Li et al. have recently demonstrated distinct roles for ATM and *Abl* in the oxidative stress response and that ATM and *Abl* differentially regulate osteoblast expression of PKC δ [28]. We demonstrated that the improved colony formation following supplementation with NAC was diminished in *Atm*KO-derived cultures. Thus, the possibility exists that irreversible damage by oxidative stress had already altered the proliferative potential of *Atm*KO-derived progenitor cells or that an additional molecular defect(s), other than the oxidative stress response, is involved.

IGF plays important roles in bone growth and metabolism [29–31]. This has been supported by genetic approaches in mice [32–35]. *ATM* deficiency downregulates the transcription of the *IGF1R* gene [36], and we found, in fact, that the expression of IGF1R, as well as the responsiveness to IGF, was decreased in marrow stromal cells of *Atm*KO mice. These results indicate that defective IGF signaling may be involved in the impaired bone formation observed in *Atm*KO mice. In addition, since serum deprivation induces oxidative stress, due mainly to loss of IGF [37], the connection between IGF activity and oxidative stress may be an interesting relationship warranting further investigation.

In conclusion, we demonstrate that *Atm*KO mice present an osteopenic phenotype as early as 10 weeks, apparently due to decreased bone-marrow-derived mesenchymal progenitors. This decline in mesenchymal progenitors may be the result of decreased expression of IGF1R, an important regulator of proliferation. The *Atm*KO mouse model may be a useful tool for further studies of senile osteoporosis.

Acknowledgments

The authors thank Drs. Yoshiko Masuda and Aya Sasaki for technical assistance in bone analyses; Miho Kamiya, Makiko Matsuura, and Kumi Tsutsumi for in vitro experiments and genotyping; Dr. Kazuhito Naka for advise in analyses of protein expression; and Dr. Akira Matsuura for critical reading of the manuscript. This study was supported in part by a grant from the Program for Promotion of Fundamental Studies in Health Sciences of the Organiza-

tion for Pharmaceutical Safety and Research of Japan and by a Research Grant for Longevity Sciences from the Ministry of Health, Labor and Welfare.

References

- [1] Bilezikian JP, Raisz LG, Rodan GA, editors. Principles of bone biology. San Diego, CA: Academic Press; 2002.
- [2] Favus MJ, editor. Primer on the metabolic bone diseases and disorders of mineral metabolism. American Society for Bone and Mineral Research; 2003.
- [3] Hasty P, Vijg J. Accelerating aging by mouse reverse genetics: a rational approach to understanding longevity. *Aging Cell* 2004;3:55–65.
- [4] Tyner SD, Venkatachalam S, Choi J, Jones S, Ghebranious N, Igelmann H, et al. p53 mutant mice that display early ageing-associated phenotypes. *Nature* 2002;415:45–53.
- [5] Kuro-o M, Matsumura Y, Aizawa H, Kawaguchi H, Suga T, Utsugi T, et al. Mutation of the mouse *klotho* gene leads to a syndrome resembling ageing. *Nature* 1997;390:45–51.
- [6] Lavin MF, Shiloh Y. The genetic defect in ataxia-telangiectasia. *Annu Rev Immunol* 1997;15:177–202.
- [7] Barlow C, Hirotsune S, Paylor R, Liyanage M, Eckhaus M, Collins F, et al. *Atm*-deficient mice: a paradigm of ataxia telangiectasia. *Cell* 1996;86:159–71.
- [8] Elson A, Wang Y, Daugherty CJ, Morton CC, Zhou F, Campos-Torres J, et al. Pleiotropic defects in ataxia-telangiectasia protein-deficient mice. *Proc Natl Acad Sci U S A* 1996;93:13084–9.
- [9] Xu Y, Ashley T, Brainerd EE, Bronson RT, Meyn MS, Baltimore D. Targeted disruption of *ATM* leads to growth retardation, chromosomal fragmentation during meiosis, immune defects, and thymic lymphoma. *Genes Dev* 1996;10:2411–22.
- [10] Rotman G, Shiloh Y. *ATM*: from gene to function. *Hum Mol Genet* 1998;7:1555–63.
- [11] Shiloh Y. *ATM* and related protein kinases: safeguarding genome integrity. *Nat Rev Cancer* 2003;3:155–68.
- [12] Liao MJ, Van Dyke T. Critical role for *Atm* in suppressing V(D)J recombination-driven thymic lymphoma. *Genes Dev* 1999;13:1246–50.
- [13] Shibata T, Shira-Ishi A, Sato T, Masaki T, Masuda A, Hishiya A, et al. Vitamin D hormone inhibits osteoclastogenesis in vivo by decreasing the pool of osteoclast precursors in bone marrow. *J Bone Miner Res* 2002;17:622–9.
- [14] Jilka RL, Weinstein RS, Takahashi K, Parfitt AM, Manolagas SC. Linkage of decreased bone mass with impaired osteoblastogenesis in a murine model of accelerated senescence. *J Clin Invest* 1996;97:1732–40.
- [15] Jochum W, David JP, Elliott C, Wutz A, Plenck Jr H, Matsuo K, et al. Increased bone formation and osteosclerosis in mice overexpressing the transcription factor *Fra-1*. *Nat Med* 2000;6:980–4.
- [16] Tsuji T, Hughes FJ, McCulloch CA, Melcher AH. Effects of donor age on osteogenic cells of rat bone marrow in vitro. *Mech Ageing Dev* 1990;51:121–32.
- [17] Kahn A, Gibbons R, Perkins S, Gazit D. Age-related bone loss. A hypothesis and initial assessment in mice. *Clin Orthop* 1995;69–75.
- [18] Bergman RJ, Gazit D, Kahn AJ, Gruber H, McDougall S, Hahn TJ. Age-related changes in osteogenic stem cells in mice. *J Bone Miner Res* 1996;11:568–77.
- [19] D'Ippolito G, Schiller PC, Ricordi C, Roos BA, Howard GA. Age-related osteogenic potential of mesenchymal stromal stem cells from human vertebral bone marrow. *J Bone Miner Res* 1999;14:1115–22.
- [20] Halloran BP, Ferguson VL, Simske SJ, Burghardt A, Venton LL, Majumdar S. Changes in bone structure and mass with advancing age in the male *C57BL/6J* mouse. *J Bone Miner Res* 2002;17:1044–50.
- [21] Bonyadi M, Waldman SD, Liu D, Aubin JE, Grynbas MD, Stanford WL. Mesenchymal progenitor self-renewal deficiency leads to age-dependent osteoporosis in *Sca-1/Ly-6A* null mice. *Proc Natl Acad Sci U S A* 2003;100:5840–5.
- [22] Peter Y, Rotman G, Lotem J, Elson A, Shiloh Y, Groner Y. Elevated Cu/Zn-SOD exacerbates radiation sensitivity and hematopoietic abnormalities of *Atm*-deficient mice. *EMBO J* 2001;20:1538–46.
- [23] Calvi LM, Adams GB, Weibrecht KW, Weber JM, Olson DP, Knight MC, et al. Osteoblastic cells regulate the haematopoietic stem cell niche. *Nature* 2003;425:841–6.
- [24] Chaturvedi P, Eng WK, Zhu Y, Mattern MR, Mishra R, Hurler MR, et al. Mammalian *Chk2* is a downstream effector of the *ATM*-dependent DNA damage checkpoint pathway. *Oncogene* 1999;18:4047–54.
- [25] Takai H, Naka K, Okada Y, Watanabe M, Harada N, Saito S, et al. *Chk2*-deficient mice exhibit radioresistance and defective p53-mediated transcription. *EMBO J* 2002;21:5195–205.
- [26] Sakai A, Sakata T, Tanaka S, Okazaki R, Kunugita N, Norimura T, et al. Disruption of the p53 gene results in preserved trabecular bone mass and bone formation after mechanical unloading. *J Bone Miner Res* 2002;17:119–27.
- [27] Li B, Boast S, de los Santos K, Schieren I, Quiroz M, Teitelbaum SL, et al. Mice deficient in *Abl* are osteoporotic and have defects in osteoblast maturation. *Nat Genet* 2000;24:304–8.
- [28] Li B, Wang X, Rasheed N, Hu Y, Boast S, Ishii T, et al. Distinct roles of *c-Abl* and *Atm* in oxidative stress response are mediated by protein kinase C delta. *Genes Dev* 2004;18:1824–37.
- [29] Baylink DJ, Finkelman RD, Mohan S. Growth factors to stimulate bone formation. *J Bone Miner Res* 1993;8(Suppl. 2):S565–72.
- [30] Delany AM, Pash JM, Canalis E. Cellular and clinical perspectives on skeletal insulin-like growth factor I. *J Cell Biochem* 1994;55:328–33.
- [31] Hayden JM, Mohan S, Baylink DJ. The insulin-like growth factor system and the coupling of formation to resorption. *Bone* 1995;17:938–8S.
- [32] Zhang M, Xuan S, Bouxsein ML, von Stechow D, Akeno N, Faugere MC, et al. Osteoblast-specific knockout of the insulin-like growth factor (IGF) receptor gene reveals an essential role of IGF signaling in bone matrix mineralization. *J Biol Chem* 2002;277:44005–12.
- [33] Devlin RD, Du Z, Buccilli V, Jorgetti V, Canalis E. Transgenic mice overexpressing insulin-like growth factor binding protein-5 display transiently decreased osteoblastic function and osteopenia. *Endocrinology* 2002;143:3955–62.
- [34] Bikle DD, Sakata T, Leary C, Elalieh H, Ginzinger D, Rosen CJ, et al. Insulin-like growth factor I is required for the anabolic actions of parathyroid hormone on mouse bone. *J Bone Miner Res* 2002;17:1570–8.
- [35] Woitge HW, Kream BE. Calvariae from fetal mice with a disrupted *Igf1* gene have reduced rates of collagen synthesis but maintain responsiveness to glucocorticoids. *J Bone Miner Res* 2000;15:1956–64.
- [36] Peretz S, Jensen R, Baserga R, Glazer PM. *ATM*-dependent expression of the insulin-like growth factor-I receptor in a pathway regulating radiation response. *Proc Natl Acad Sci U S A* 2001;98:1676–81.
- [37] Busiguina S, Fernandez AM, Barrios V, Clark R, Tolbert DL, Berciano J, et al. Neurodegeneration is associated to changes in serum insulin-like growth factors. *Neurobiol Dis* 2000;7:657–65.